Molecular dynamics simulation of deposition of amorphous carbon films on sapphire surfaces

Qiang Yue[1*] , Takayoshi Yokoya[2] , Yuji Muraoka[2 *]

[1]*Graduate School of Natural Science and Technology, Okayama University, 3-1-1 Tsushima-naka, Tsushima, Kita-ku, Okayama, 700-8530, Japan*

[2]*Research Institute for Interdisciplinary Science, Okayama University, 3-1-1 Tsushima-naka, Tsushima, Kita-ku, Okayama, 700-8530, Japan*

[*]E-mail: p37126c5@s.okayama-u.ac.jp, ymuraoka@cc.okayama-u.ac.jp

Abstract

The growth of amorphous carbon films on a sapphire surface was investigated using classical molecular dynamics simulation. The kinetic energy of carbon particles was set as 10 eV and ReaxFF potential was used to express the interaction between different kinds of particles. The results of the temperature distribution in both deposition time and deposition space are reported. Simulation results reveal that the grown amorphous carbon film consists of four regions, namely interlayer, low density, stable growth, and surface regions. In the interlayer region, the interlayer between substrate and pure carbon film is formed. In the low density region, a pure carbon film is grown while the film density decreases initially and then increases. In the stable growth region, the film density remains almost constant. The film density decreases rapidly in the surface region. The radial distribution function (RDF) analysis suggests that a structure similar to that of diamond exists in the stable growth region of the film. The lower film density in the low density and surface regions was interpreted to indicate the existence of abundant sp^1 chain structures, which is supported by the depth profile of the sp fractions. The present results are in good agreement with previous experimental and simulation results and demonstrate the

suitability of the ReaxFF potential in the simulation of amorphous carbon growth on sapphire substrate. Our study provides a good starting point for the simulation study of amorphous carbon films on sapphire substrates.

Keywords: Amorphous carbon; Sapphire substrate; Molecular dynamics simulation; Empirical potential

1 1. Introduction

2 Amorphous carbon, especially diamond-like carbon with high sp^3 content, exhibits unique
3 properties, such as high hardness, low friction coefficient, chemical stability, and
4 biocompatibility [1,2,3]. These properties change accordingly due to the difference of the sp^3
5 content in amorphous carbon. Research methods on the properties of amorphous carbon can be
6 broadly divided into experiment and simulation. Experimentally, the properties of amorphous
7 carbon film have been studied as deposited on substrates such as silicon [4] and sapphire [5,6,7].

8 Classical molecular dynamics (CMD) simulation can study the properties of amorphous
9 carbon at the atomic level, providing microscopic information unattainable by experiments, and
10 can be used as an auxiliary means to explain phenomena observed in experiments. Moreover,
11 CMD simulation can obtain results under ideal conditions, allowing qualitative comparison
12 with experiments.

13 Numerous researchers have studied amorphous carbon using CMD methods. Jäger and Albe
14 [8] performed deposition simulation on a diamond (111) substrate and found that the amount of
15 sp^3 in the simulated carbon film could be increased using a larger carbon-carbon interaction
16 cutoff value. Wang and Komvopoulos [9] performed deposition simulation on the surface of
17 silicon (100) substrates. Their simulations showed the existence of multilayer structures in
18 carbon films with a thickness of 20 Å and found that the particle energy of ~ 80 eV produced
19 the film with the highest sp^3 content. Murakami et al. [10] deposited CH_3 and CH particles on
20 the surface of amorphous carbon substrates and found that the presence of hydrogen promoted
21 the formation of sp^3 structures. Gou et al. [11] set the initial temperature of the SiC (001)
22 substrates at 300 K and used CH_3 particles with an energy of 50-150 eV to perform deposition
23 simulations. Their simulations showed that increasing the energy of incoming particles
24 decreased the deposition rate of hydrogen atoms, while having little effects on the deposition

rate of carbon atoms. Furthermore, previous simulations have shown that the properties of carbon films can be affected by the substrate. Deposited carbon films on diamond substrates by CMD simulation generally have one bulk layer of nearly constant density, which is unaffected by the kinetic energies of incident particles [8,12]. In contrast, the CMD simulations by Huang et al. [13] showed that the densities of the amorphous carbon films deposited on silicon (001) surface depend on particle energies and the densities remain nearly constant in the bulk layer only when the incident energies are greater than 40 eV. Moreover, although sapphire substrates are widely used in carbon film deposition experiments, related simulation studies have not been performed to date.

This study aimed to use carbon particles with low kinetic energy to deposit amorphous carbon films on sapphire substrates to investigate the microscopic growth process of film using CMD simulation. The different growth stages and the depth dependence of sp^3 ratio, density, and components of the film were revealed. The results of this study will guide future simulation studies of the deposition of amorphous carbon films on sapphire substrates.

2. Molecular dynamics simulation process

LAMMPS code [14,15,16] was used to implement molecular dynamics simulations and OVITO software [17] was used to visualize the simulation results. To accurately describe the interaction forces between carbon, oxygen, and aluminum atoms, the reactive force-field (ReaxFF) interatomic potential developed by Hong and Van Duin [18] was used, which was found to be only suitable potential for our simulation. As a novel empirical bond-order potential, ReaxFF can implicitly describe chemical bonding without expensive quantum mechanics calculations [19]. As this potential was used to simulate the deposition of amorphous carbon

films for the first time, it was necessary to test whether this potential could correctly describe the relevant properties of carbon films. Thus, the preliminary simulations were conducted using the liquid quenching method [20]. By changing the number of particles in the simulation box with fixed volume, the density of the system varied between 1.42 and 2.99 g/cm^3. As shown in Fig. 1(a), 1600 carbon atoms were randomly placed inside a three-dimensional periodic cubic box (size: 22 Å × 22 Å × 22 Å). The canonical (NVT) ensemble was used, and the temperature was controlled by Langevin thermostat [21] with a time step of 0.1 fs. First, the system was equilibrated at 300 K for 5 ps and then slowly heated to 8000 K within 15 ps. The system was then maintained in the liquid state for 3 ps to eliminate the influence of the initial structure as much as possible. Next, the system temperature was linearly quenched to 300 K within 2 ps and finally equilibrated again at 300 K for 3 ps. The overall temperature change of this system is shown in Fig. 1(b). To judge whether the phase transition states of the systems meet expectations, the mean square displacement (MSD) was calculated. When the system is in a solid state, the MSD has an upper limit and does not change with time; when the system is in the liquid state, the MSD increases with time. Figure 1(c) shows the corresponding MSD curve, which is in good agreement with the expected state at each temperature stage. To calculate the coordination number of atoms in the simulated system, the bond cutoff distance was set as 1.85 Å. As shown in Fig. 1(d), the sp^3 content increases with density, which is qualitatively consistent with the results based on simulations using other potentials [22-24] and experiments [25,26]. This suggests that the ReaxFF potential used in this study accounts well for changes in sp^3 content of amorphous carbon with different densities.

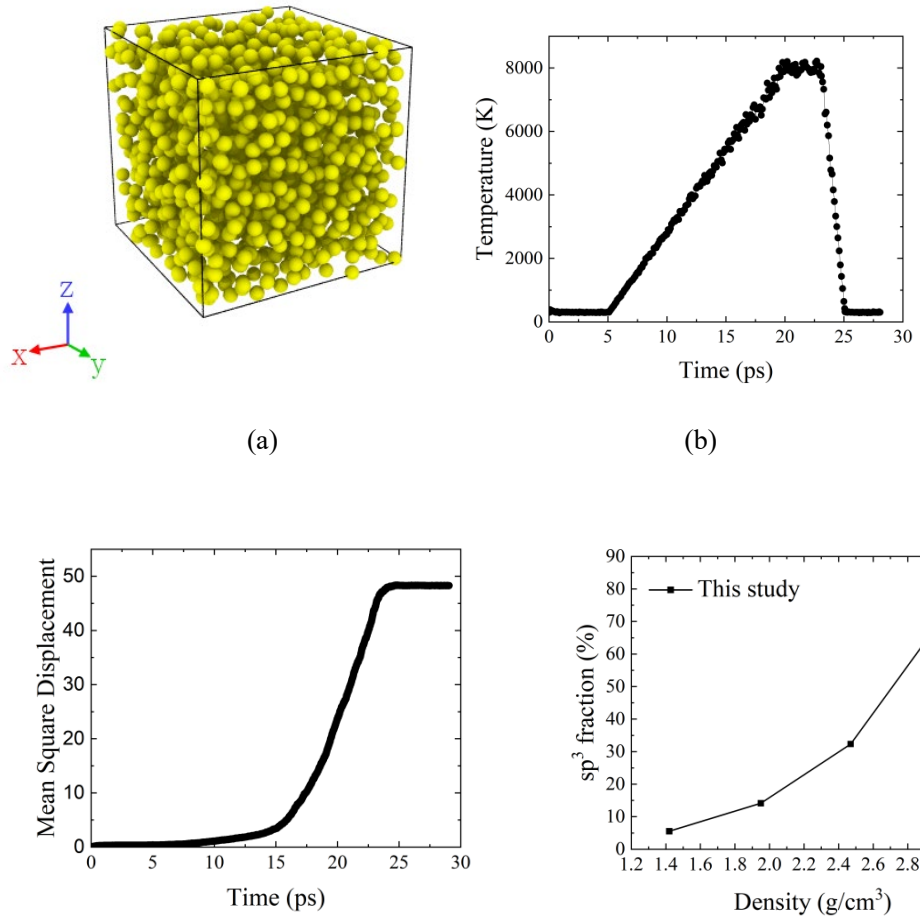

Fig. 1. (a) Model used for liquid quenching simulation. (b) Time dependence of the overall temperature in the system. (c) Time dependence of the mean square displacement in the system. (d) Change of sp^3 fraction as a function of density in the amorphous carbon films.

The three-dimensional simulation box is shown in Fig. 2. The space group of the conventional cell of sapphire (α-Al_2O_3) crystal is R-3C, and the lattice constant are a = b = 4.805 Å, c = 13.1163 Å, $\alpha = \beta = 90°$, and $\gamma = 120°$ [27]. To avoid overlap of substrate atoms, the conventional cell is orthogonalized using the free and open-source command-line program ATOMSK [28]. The size of the sapphire substrate is 24.9678 Å × 24.025 Å × 26.2326 Å and the Miller index of the upper surface is (0001). Atoms are fixed within the 2.186 Å thickness at the bottom of the substrate to mimic an infinitely thick bulk substrate. Above the region of fixed atoms, the temperature of atoms within a thickness of 10.9303 Å were kept at 300 K by Berendsen thermostat [29]. The remaining region of substrate and the deposition

region of the amorphous carbon film, except the top region with a thickness of 5 Å, was divided into two parts [8]: the atoms in the cylindrical region with a radius of 11 Å were unconstrained, and the atoms in the remaining region were also kept at 300 K by Berendsen thermostat. In addition, the atom groups except that corresponding to fixed region could be updated at each time step according to their positions. For deposition, 2800 carbon atoms with kinetic energy of 10 eV were randomly generated at a distance of 135 Å from the substrate surface and were deposited sequentially. According to the relationship between kinetic energy and velocity, the velocity of a single carbon particle was calculated to be 126.78 Å/ps. The successive incident interval of carbon atoms was set as 10 ps, and the time step was set as 0.25 fs [30]. Periodic boundary conditions were applied in the x and y directions. The preliminary simulations showed that the above settings could effectively suppress the heat accumulation caused by the incident carbon atoms. After the deposition, the system was relaxed for 100 ps to obtain the final stable structure. Simulations using ReaxFF potential incur large computational cost. Thus, studying all the cases using different energies is impractical. The kinetic energy of 10 eV is the smallest one used in most previous simulation studies. As our report provides the first result of a deposition simulation for carbon film on sapphire substrate, one deposition model was considered worthy of study.

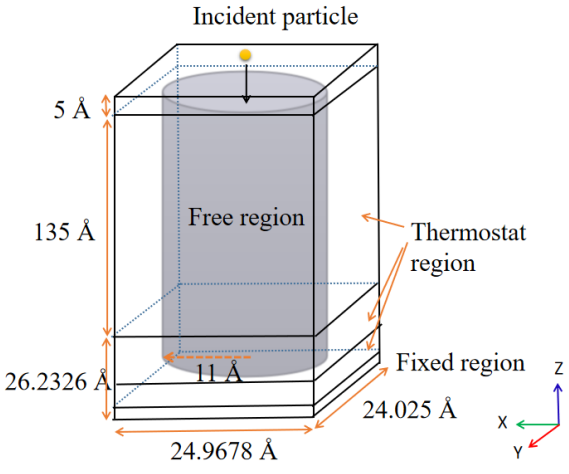

Fig. 2. Film deposition model in our simulation.

When analyzing properties of the simulated system, along the normal direction of the substrate surface, the corresponding average values in the thin slices with a thickness of 2.18605 Å were calculated sequentially, to analyze the distribution of the density, sp contents, temperature, and the different atomic compositions. For the stable growth region of carbon film, the radial distribution function (RDF) was analyzed.

3. Results and discussion

The overall temperature change during deposition is shown in Fig. 3(a). When the incident carbon atoms bombard the surface of the system, the thermal energy converted from the kinetic energy causes the temperature of the system to rise instantaneously. Afterwards, owing to the effective dissipation of heat, the temperature of the system decreases again. In initial stage of deposition, many particles, mainly oxygen atoms, escape from the system, as mentioned later. This makes the temperature of the system unstable. In the growth stage of pure amorphous carbon film, the temperature of the system after quenching is basically maintained at approximately 350 K. Fig. 3(b) shows the temperature distribution in space along Z direction after completing deposition (before relaxation again). The position of the initial substrate surface is the origin, and the positive direction of z-axis is the growth direction of film. As shown in Fig. 3(b), the temperature essentially remains below 400 K at various depths of the system after deposition. This indicates little possibility that the film properties are affected by temperature [31,32]. The temperature distributions in both time and space show that our model does well to inhibit the accumulation of heat. Furthermore, to the best of our knowledge, no simulation study on the temperature distribution in both time and space has been reported by other researchers. Our study is the first to provide related results.

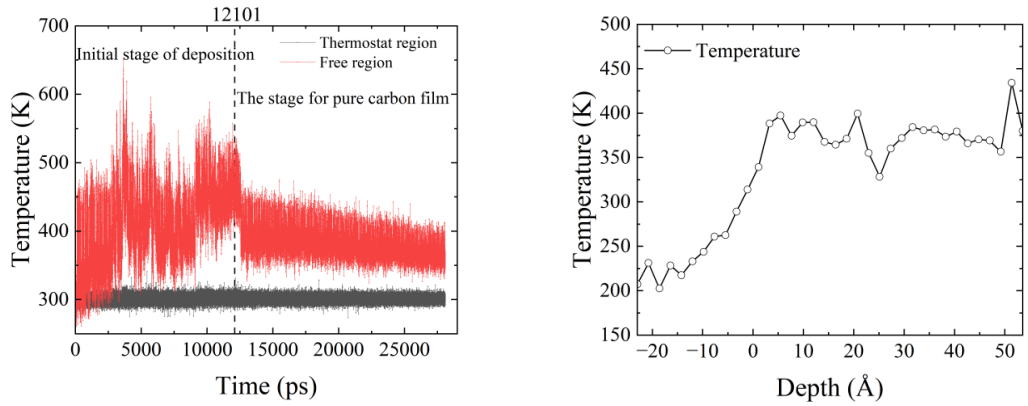

(a) (b)

Fig. 3. (a) Temperature change of free (black dotted line) and thermostat (red dotted line) regions during deposition. (b) Depth dependence of the system temperature after film deposition.

Figure 4 shows the different film growth stages corresponding to different deposition amounts. In the initial deposition stage (Fig. 4(a)), some carbon atoms penetrate the interior of the substrate, and some are rebounded from the substrate. Furthermore, oxygen atoms existing in the substrate can also escape from the system due to the collision of deposited carbon particles. As the deposition proceeds, the penetration of carbon atoms and the etching of oxygen atoms by carbon atoms gradually intensify, and an interlayer progressively forms between the substrate and pure carbon film regions (Fig. 4(b)). Experimentally, amorphous carbon films have been found to adhere well to sapphire substrates [5,6,7]. This is plausible owing to the existence of an interlayer between film and substrate. The experimental results are well explained by our simulation result. Furthermore, Fig. 4(b) shows that some deposited carbon particles form short chains during the formation of the interlayer. After the formation of the interlayer, a pure amorphous carbon film begins to grow. Interestingly, as shown in Fig. 4(c), many long carbon chains emerge and intertwine to form a sparse network structure, which creates many voids in the film. Fig. 4(d) shows the stage of stable film growth with a constant density. In this stage, the length and number of carbon chains decrease dramatically. The carbon

chains tend to bend and intertwine to form a dense network structure. A similar growth phenomenon is reported in a previous simulation study [33].

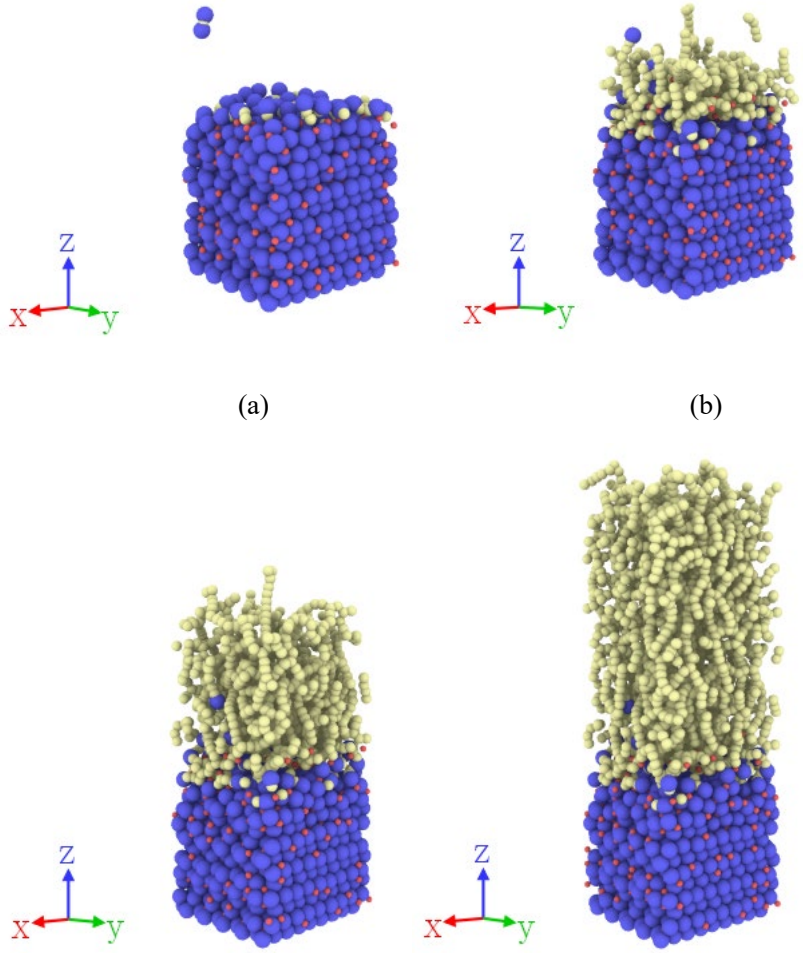

Fig. 4. Illustration of the film deposition at different stages. Aluminum, oxygen, and carbon atoms are represented by red, blue, and yellow balls, respectively. (a) Initial stage of deposition. (b) Stage of interlayer formation. (c) Stage of low density film formation. (d) Final stage of the deposited film.

Fig. 5(a) shows the distribution of different atoms in the system along the z-axis. Because the microstructure is very small, the number ratio of oxygen atoms to aluminum atoms near bottom boundary does not meet the stoichiometric ratio, which is 3:2 in sapphire crystal. At the z coordinate of -7.65 Å, the perfect crystal structure of sapphire begins degrade although number ratio of carbon atoms is zero, and the formation of the interlayer starts. Due to the penetration of carbon atoms, the number ratio of oxygen and aluminum atoms drops rapidly

and the number ratio of carbon atoms rises rapidly. However, because many oxygen atoms are etched away, their number ratio decreases faster than that of aluminum atoms. Finally, the number ratio of oxygen and aluminum atoms drops to almost zero, corresponding to the end of the formation of the interlayer. The thickness of the interlayer is about 21.86 Å. Notably, the existence of an interlayer has been verified experimentally when amorphous carbon films are deposited on silicon substrates [4,34,35]. The formation of an interlayer seems to be a common phenomenon in the experimental deposition of amorphous carbon films on different substrates.

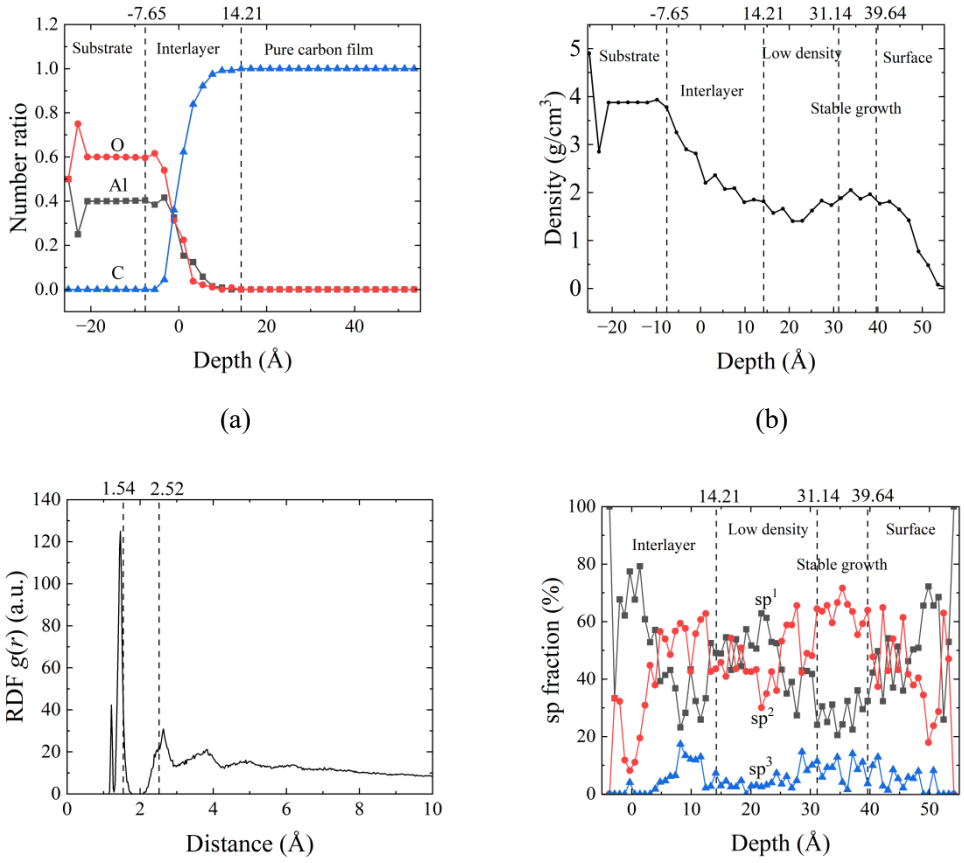

Fig. 5. (a) Number ratio of different atoms as a function of film depth. (b) Depth profile of the film density. (c) RDF of amorphous carbon film in the stable growth region. The dashed lines located at 1.52 Å and 2.54 Å correspond to the 1st and 2nd nearest neighboring peaks of diamond. (d) Depth profile of the sp fractions in the stable growth region of amorphous carbon.

Figure 5(b) shows the density distribution in space. The density in the interlayer region gradually decreases from 3.87 g/cm^3 to 1.81 g/cm^3. As the film growth continues, the pure

carbon film starts to form, and the film density continues to decrease from 1.81 g/cm^3 to 1.40 g/cm^3 and then increases up to 1.88 g/cm^3. This region is denoted as the low density region. The decrease in the film density in this region is due to the formation of the sparse network of long, interlinked carbon chains (Fig. 4(c)). After the low density region is the stable growth region. In this relatively thin region, the amorphous carbon film has an approximately constant density of 1.94 g/cm^3. At the surface of the film, the density starts to decrease again. This is because the sparse chain structures had become the main morphology. The existence of a surface layer with a lower density has been reported experimentally [4,35]. Furthermore, as the film is further deposited, only the thickness of the stable growth region increases, while that of the other regions (substrate, interlayer, and low density regions) remain unchanged.

The structure of the film in stable growth region was analyzed using the RDF $g(r)$ given by Eq. (1):

$$g(r) = \frac{dN}{\rho \cdot 4\pi r^2 dr} \qquad (1)$$

where ρ is the average number density of the system, and dN is the number of particles in the spherical shell between r and $r+dr$ from the central reference atom. Figure 5(c) is the RDF of the amorphous carbon film in the stable growth region. For reference, the dashed lines at 1.52 Å and 2.54 Å were added, which correspond to the first and second nearest neighboring peaks of diamond. The curves in the figure show the typical amorphous structure features of short-range order and long-range disorder. The positions of the first and second nearest neighboring peaks are 1.46 Å and 2.64 Å, which are close to those of diamond. This suggests the existence of a structure similar to that of diamond in this region of the film. A small, very narrow peak appears on the left side of the first nearest peak, which may be caused by a deficiency of the ReaxFF potential used. The position corresponding to the valley (1.85 Å) between the first

neighbor and the second neighbor peak was used as the bond cutoff distance of carbon atoms. The coordination number and hybridization state of each carbon atom were determined by the number of particles within this cutoff distance.

Fig. 5(d) shows the sp fractions in the film as a function of film depth. In the interlayer region, sp^1 and sp^2 bonding are dominant. The sp^1 fraction tends to increase slightly and the sp^2 fraction tends to decrease while the sp^3 fraction remains unchanged in the low density region. In the stable growth region, the sp fractions are almost constant. In the surface region, the sp^1 fraction tends to increase towards the uppermost part of the film surface. The relatively higher sp^1 fraction in the low density and surface growth regions can be explained based on growth morphology (Fig. 4(c), 4(d)). Maharizi et al. [6] reported the experimental result of amorphous carbon films deposited on sapphire substrates by chemical vapor growth. They observed a constant region of the concentration of diamond bonds (sp^3 fraction) inside the amorphous carbon film with a thickness of 400 nm. Our simulation result is qualitatively consistent with their experimental finding.

4. Conclusions

In this study, CMD simulations were used to analyze the deposition of carbon particles of 10 eV on sapphire substrates under ideal conditions. The temperature distribution in deposition time and space demonstrated that the model could effectively inhibit heat accumulation during deposition. ReaxFF potential was used in this simulation and the related results were qualitatively consistent with those of previously reported experiments and simulation results obtained using other potentials. The CMD simulations revealed that the grown film consists of four regions, namely interlayer, low density, stable growth, and surface regions. The first region

contained the interlayer formed between the substrate and pure carbon film. In the low density region, a pure carbon film was grown as the film density decreased initially and then increased. In the stable growth region, the film density was almost constant. A further decrease in film density was observed in the surface region. The existence of the interlayer was consistent with reported experimental results, where amorphous carbon adhered well to the sapphire substrate. RDF analysis suggests that a structure similar to that of diamond exists in the stable growth region. The lower film densities in the low density and surface regions were interpreted as the main presence of sp^1 chain structures, which was supported by the results of the sp fractions with film depth. The present results were basically consistent with those of previously reported experimental and simulation studies. Furthermore, our results demonstrate the applicability of the ReaxFF potential in the simulation of amorphous carbon growth on sapphire substrate. We believe that our study will accelerate the simulation research of amorphous carbon growth on sapphire substrate using the ReaxFF potential.

CRediT author statement

Qiang Yue: Methodology, Investigation, Software, Data curation, Writing - Original draft preparation. **Takayoshi Yokoya:** Writing - Reviewing and Editing. **Yuji Muraoka:** Conceptualization, Supervision, Writing - Reviewing and Editing.

Declaration of interests

The authors declare that they have no known competing financial interests or personal relationships that could have appeared to influence the work reported in this paper.

Acknowledgment

We would like to express our gratitude to Professor Kenji Tsuruta for kind suggestions on selecting the potential, and we further thank Dr. Axel Kohlmeyer for prompt and detailed guidance on using LAMMPS. This work was supported by JSPS KAKENHI [grant number JP21H01624].

References

[1] K. Bewilogua, D. Hofmann, History of diamond-like carbon films — From first experiments to worldwide applications, Surf. Coat. Tech. 242 (2014) 214-225. https://doi.org/10.1016/j.surfcoat.2014.01.031.

[2] A. Tyagi, R. S. Walia, Q. Murtaza, S. M. Pandey, P. K. Tyagi, B. Bajaj, A critical review of diamond like carbon coating for wear resistance applications, Int. J. Refract. Met. H. 78 (2019) 107-122. https://doi.org/10.1016/j.ijrmhm.2018.09.006.

[3] R. Hauert, K. Thorwarth, G. Thorwarth, An overview on diamond-like carbon coatings in medical applications, Surf. Coat. Tech. 233 (2013) 119-130. https://doi.org/10.1016/j.surfcoat.2013.04.015.

[4] G. M. Pharr, D. L. Callahan, S. D. McAdams, T. Y. Tsui, S. Anders, A. Anders, J. W. Ager III, I. G. Brown, C. S. Bhatia, S. R. P. Silva, J. Robertson, Hardness, elastic modulus, and structure of very hard carbon films produced by cathodic‐arc deposition with substrate pulse biasing, Appl. Phys. Lett. 68 (1996) 779-781. https://doi.org/10.1063/1.116530.

[5] H. Yoshinaka, S. Inubushi,T. Wakita, T. Yokoya, Y. Muraoka, Formation of Q-carbon by adjusting sp3 content in diamond-like carbon films and laser energy density of pulsed laser annealing, Carbon, 167 (2020) 504-511. https://doi.org/10.1016/j.carbon.2020.06.025.

[6] M. Maharizi, D. Peleg, A. Seidman, N. Croitoru, The influence of substrate and film thickness on the morphology and diamond bond formation during the growth of amorphous diamond-like carbon (DLC) films, J. Optoelectron. Adv. Mater. 1 (1999) 65-68.

[7] J. Narayan, P. Joshi, J. Smith, W. Gao, W. J. Weber, R. J. Narayan, Q-carbon as a new radiation-resistant material, Carbon. 186 (2022) 253-261. https://doi.org/10.1016/j.carbon.2021.10.006.

[8] H. U. Jäger, K. Albe, Molecular-dynamics simulations of steady-state growth of ion-deposited tetrahedral amorphous carbon films, J. Appl. Phys. 88 (2000) 1129-1135. https://doi.org/10.1063/1.373787.

[9] S. Wang, K. Komvopoulos, Structure evolution during deposition and thermal annealing of amorphous carbon ultrathin films investigated by molecular dynamics simulations, Sci. Rep. 10 (2020) 8089. https://doi.org/10.1038/s41598-020-64625-w.

[10] Y. Murakami, S. Horiguchi, S. Hamaguchi, Molecular dynamics simulation of the formation of sp^3 hybridized bonds in hydrogenated diamondlike carbon deposition processes, Phys. Rev. E. 81 (2010) 041602. https://doi.org/10.1103/PhysRevE.81.041602.

[11] F. Gou, M. Chuanliang, Z. T. Zhouling, Q. Qian, Hydrocarbon film growth by energetic CH^3 molecule impact on SiC (0 0 1) surface, Appl. Surf. Sci. 253 (2007) 8517-8523. https://doi.org/10.1016/j.apsusc.2007.04.023.

[12] A.Y. Belov, H. U. Jäger, Simulation of the non-equilibrium processes for tetrahedral amorphous carbon: Deposition and structural relaxation, Nucl Instrum Meth B. 202 (2003) 242 – 248. https://doi.org/10.1016/S0168-583X(02)01864-5.

[13] D. Huang, J. Pu, Z. Lu, Q. Xue. Microstructure and surface roughness of graphite-like carbon films deposited on silicon substrate by molecular dynamic simulation, Surf. Interface Anal. 44 (2012) 837-843. https://doi.org/10.1002/sia.4898.

[14] A. P. Thompson, H. M. Aktulga, R. Berger, D. S. Bolintineanu, W. M. Brown, P. S. Crozier, P. J. in't Veld, A. Kohlmeyer, S. G. Moore, T. D. Nguyen, R. Shan, M. J. Stevens, J. Tranchida, C. Trott, S. J. Plimpton, LAMMPS - a flexible simulation tool for particle-based materials modeling at the atomic, meso, and continuum scales, Comp. Phys. Comm, 271 (2022) 10817. https://doi.org/10.1016/j.cpc.2021.108171.

[15] H. M. Aktulga, J. C. Fogarty, S. A. Pandit, A. Y. Grama, Parallel reactive molecular dynamics: Numerical methods and algorithmic techniques, Parallel. Comput. 38 (2012) 245-259. https://doi.org/10.1016/j.parco.2011.08.005.

[16] S. Plimpton, Fast Parallel Algorithms for Short-Range Molecular Dynamics, J. Comp. Phys, 117 (1995) 1-19. https://doi.org/10.1006/jcph.1995.1039.

[17] A. Stukowski, Visualization and analysis of atomistic simulation data with OVITO–the Open Visualization Tool, Modelling Simul. Mater. Sci. Eng. 18 (2010) 015012. https://dx.doi.org/10.1088/0965-0393/18/1/015012.

[18] S. Hong, A. C. T. Van Duin, Atomistic-Scale Analysis of Carbon Coating and Its Effect on the Oxidation of Aluminum Nanoparticles by ReaxFF-Molecular Dynamics Simulations, J. Phys. Chem. C. 120 (2016) 9464-9474. https://doi.org/10.1021/acs.jpcc.6b00786.

[19] T. P. Senftle, S. Hong, M. M. Islam, S. B. Kylasa, Y. Zheng, Y. K. Shin, C. Junkermeier, R. Engel-Herbert, M. J. Janik, H. M. Aktulga, T. Verstraelen, A. Grama, A. C. T. van Duin, The ReaxFF reactive force-field: development, applications and future directions, NPJ Comput Mater. 2 (2016) 15011. https://doi.org/10.1038/npjcompumats.2015.11.

[20] N. A. Marks, Evidence for subpicosecond thermal spikes in the formation of tetrahedral amorphous carbon, Phys. Rev. B. 56 (1997) 2441-2446. https://link.aps.org/doi/10.1103/PhysRevB.56.2441.

[21] T. Schneider, E. Stoll, Molecular-dynamics study of a three-dimensional one-component model for distortive phase transitions, Phys. Rev. B. 17 (1978) 1302-1322. https://link.aps.org/doi/10.1103/PhysRevB.17.1302.

[22] C. D. Tomas, I. Suarez-Martinez, N. A. Marks, Graphitization of amorphous carbons: A comparative study of interatomic potentials, Carbon. 109 (2016) 681-693. https://doi.org/10.1016/j.carbon.2016.08.024.

[23] C. D. Tomas, A. Aghajamali, J. L. Jones, D. J. Lim, M. J. Lopez, I. Suarez-Martinez, N. A. Marks, Transferability in interatomic potentials for carbon, Carbon. 155 (2019) 624-634. https://doi.org/10.1016/j.carbon.2019.07.074.

[24] L. Li, M. Xu, W. Song, A. Ovcharenko, G. Zhang, D. Jia, The effect of empirical potential functions on modeling of amorphous carbon using molecular dynamics method, Appl. Surf. Sci. 286 (2013) 287-297. https://doi.org/10.1016/j.apsusc.2013.09.073.

[25] A. C. Ferrari, A. Libassi, B. K. Tanner, V. Stolojan, J. Yuan, L. M. Brown, S. E. Rodil, B. Kleinsorge, J. Robertson, Density, sp^3 fraction, and cross-sectional structure of amorphous carbon films determined by x-ray reflectivity and electron energy-loss spectroscopy, Phys. Rev. B, 62 (2000) 11089-11103. https://link.aps.org/doi/10.1103/PhysRevB.62.11089.

[26] S. Ravi, P. Silva, S. Xu, B. X. Tay, H. S. Tan, W. I. Milne, Nanocrystallites in tetrahedral amorphous carbon films, Appl. Phys. Lett. 69 (1996) 491-493. https://doi.org/10.1063/1.117763.

[27] A. Jain, S. P. Ong, G. Hautier, W. Chen, W. D. Richards, S. Dacek, S. Cholia, D. Gunter, D. Skinner, G. Ceder, K. A. Persson, Commentary: The Materials Project: A materials genome approach to accelerating materials innovation, APL. Mater. 1 (2013) 011002. https://doi.org/10.1063/1.4812323.

[28] P. Hirel, Atomsk: A tool for manipulating and converting atomic data files, Comput. Phys. Comm. 197 (2015) 212-219. https://doi.org/10.1016/j.cpc.2015.07.012.

[29] H. J. C. Berendsen, J. P. M. Postma, W. F. van Gunsteren, A. DiNola, J. R. Haak, Molecular dynamics with coupling to an external bath, J. Chem. Phys. 81 (1984) 3684-3690. https://doi.org/10.1063/1.448118.

[30] X. Li, H. Mizuseki, S. J. Pai, K. -R. Lee, Reactive molecular dynamics simulation of the amorphous carbon growth: Effect of the carbon triple bonds, Comp. Mater. Sci, 169 (2019) 109143. https://doi.org/10.1016/j.commatsci.2019.109143.

[31] M. Chhowalla, J. Robertson, C. W. Chen, S. R. P. Silva, C. A. Davis, G. A. J. Amaratunga, W. I. Milne, Influence of ion energy and substrate temperature on the optical and electronic properties of tetrahedral amorphous carbon (ta-C) films, J. Appl. Phys 81 (1997) 139-145. https://doi.org/10.1063/1.364000.

[32] Y. Lifshitz, G. D. Lempert, E. Grossman, Substantiation of subplantation model for diamondlike film growth by atomic force microscopy, Phys. Rev. Lett. 72 (1994) 2753-2756. https://doi.org/10.1103/PhysRevLett.72.2753.

[33] X. Li, P. Ke, H. Zheng, A. Wang, Structural properties and growth evolution of diamond-like carbon films with different incident energies: A molecular dynamics study, Appl. Surf. Sci. 273 (2013) 670-675. https://doi.org/10.1016/j.apsusc.2013.02.108.

[34] E. G. Gerstner, D. P. McKenzie, M. K. Puchert, P. Y. Trimbell, J. Zou, Adherent carbon film deposition by cathodic arc with implantation, J. Vac. Sci. Technol. A 13 (1995) 406-411. https://doi.org/10.1116/1.579372.

[35] C. A. Davis, G. A. J. Amaratunga, K. M. Knowles, Growth Mechanism and Cross-Sectional Structure of Tetrahedral Amorphous Carbon Thin Films, Phys Rev Lett. 80 (1998) 3280-3283. https://doi.org/10.1103/PhysRevLett.80.3280.